Inorganic Chemistry

Article

pubs.acs.org/IC

Insights into Ru-Based Molecular Water Oxidation Catalysts: Electronic and Noncovalent-Interaction Effects on Their Catalytic Activities

Lele Duan,[†] Lei Wang,[†] A. Ken Inge,[‡] Andreas Fischer,[†] Xiaodong Zou,[‡] and Licheng Sun*[,†,§]

[†]Department of Chemistry, School of Chemical Science and Engineering, KTH Royal Institute of Technology, SE-100 44 Stockholm, Sweden

[‡]Berzelii Center EXSELENT on Porous Materials and Department of Materials and Environmental Chemistry, Stockholm University, SE-106 91 Stockholm, Sweden

[§]State Key Lab of Fine Chemicals, DUT-KTH Joint Education and Research Center on Molecular Devices, Dalian University of Technology (DUT), 116024 Dalian, China

Supporting Information

ABSTRACT: A series of Ru-bda water oxidation catalysts [Ru(bda)L_2] (H_2bda = 2,2′-bipyridine-6,6′-dicarboxylic acid; L = [$HNEt_3$][3-SO_3-pyridine], **1**; 4-(EtOOC)-pyridine, **2**; 4-bromopyridine, **3**; pyridine, **4**; 4-methoxypyridine, **5**; 4-(Me_2N)-pyridine, **6**; 4-[$Ph(CH_2)_3$]-pyridine, **7**) were synthesized with electron-donating/-withdrawing groups and hydrophilic/hydrophobic groups in the axial ligands. These complexes were characterized by ^{1}H NMR spectroscopy, high-resolution mass spectrometry, elemental analysis, and electrochemistry. In addition, complexes **1** and **6** were further identified by single crystal X-ray crystallography, revealing a highly distorted octahedral configuration of the Ru coordination sphere. All of these complexes are highly active toward Ce^{IV}-driven (Ce^{IV} = $Ce(NH_4)_2(NO_3)_6$) water oxidation with oxygen evolution rates up to 119 mols of O_2 per mole of catalyst per second. Their structure−activity relationship was investigated. Electron-withdrawing and noncovalent interactions (attraction) exhibit positive effect on the catalytic activity of Ru-bda catalysts.

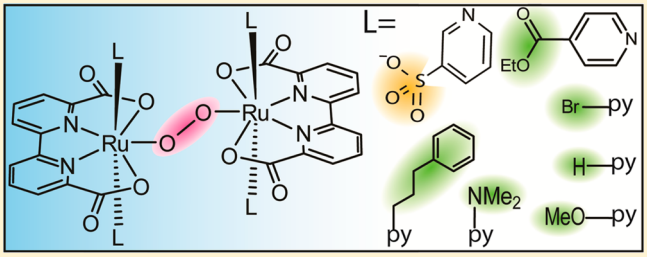

INTRODUCTION

Splitting water to hydrogen and oxygen, driven by solar energy, has long been perceived as a promising way to replace fossil fuels. One of the obstacles preventing the application of water splitting devices comes from the lack of efficient (high activity and low overpotential), robust and cost-effective catalysts for water oxidation which produces protons and electrons as starting materials for hydrogen production. Many transition metal complexes including Ir-,[1] Ru-,[2] Cu-,[3] Mn-,[4] Co-,[5] and Fe-complexes[6] have been reported capable of catalyzing water oxidation.

We recently reported a family of Ru-bda (H_2bda = 2,2′-bipyridine-6,6′-dicarboxylic acid) water oxidation catalysts [Ru(bda)L_2] (L = N-donor ligands; see Figure 1 for selected Ru-bda water oxidation catalysts **A**−**E**) that effectively catalyze Ce^{IV}-driven (Ce^{IV} = $Ce(NH_4)_2(NO_3)_6$) water oxidation, with turnover frequencies (TOFs) up to 300 per second and turnover numbers (TONs) up to 55400.[7] Mechanistic studies have revealed that (i) seven-coordinate ruthenium species are involved in the catalytic cycle, as evidenced by the isolation of a seven-coordinate Ru^{IV} dimer, and (ii) Ru-bda catalysts catalyze water oxidation via a bimolecular coupling pathway, in which the O−O bond formation step involves the coupling of two Ru^{V}═O species (Scheme 1A). The proposed reaction mechanism is represented in Scheme 2.[7b] In contrast, other mononuclear Ru water oxidation catalysts usually form six-coordinate Ru−OH/Ru═O species at the Ru +IV and +V states, and the nucleophilic attack of a water molecule on a Ru^{V}═O (or Ru^{IV}═O, see ref 2u) species forms the O−O bond (Scheme 1B).[2j] From the mechanistic point of view, Ru-bda water oxidation catalysts are largely different from other mononuclear water oxidation catalysts. It is interesting to explore this family of catalysts to gain more insights in their

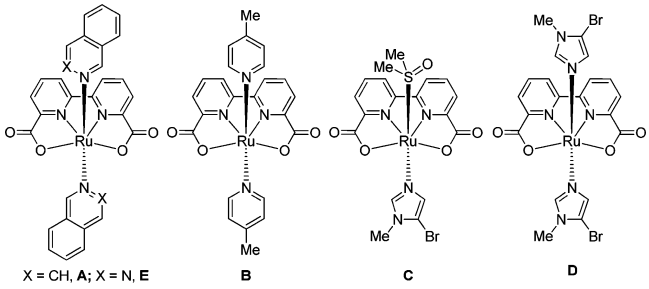

Figure 1. Selected Ru-bda water oxidation catalysts **A**−**E**.

Received: December 7, 2012
Published: June 28, 2013

   dx.doi.org/10.1021/ic302687d | *Inorg. Chem.* 2013, 52, 7844−7852

Scheme 1. Illustrations of the Intermolecular Coupling Pathway versus the Water Nucleophilic Attack Pathway and the 7-Coordinate Ru^{V}=O versus the 6-Coordinate Ru^{V}=O, Respectively

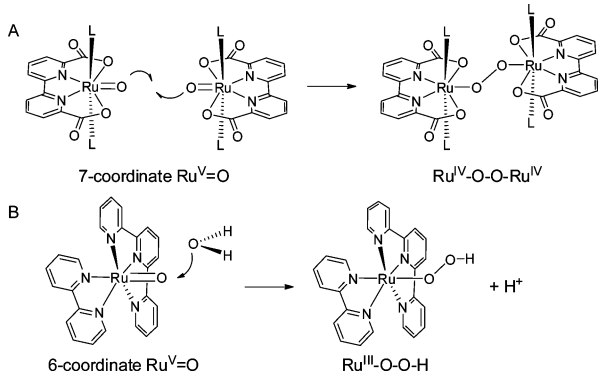

Scheme 2. Proposed Water Oxidation Mechanism by Ru-bda Catalysts with H_2O as the Seventh Ligand (Ref 7b)

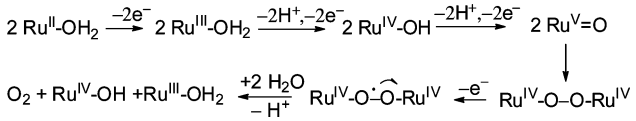

nature. Our focus in this paper is to develop efficient Ru-based water oxidation catalysts and understand the structure−activity relationship.

We have noticed that the equatorial bda ligand is essential for Ru-bda catalysts being efficient. When the bda ligand is replaced by a pda ligand (H_2pda = 1,10-phenanthroline-2,9-dicarboxylic acid), the resulting [Ru(pda)L_2] complexes catalyze water oxidation via the water nucleophilic attack pathway instead of the bimolecular coupling pathway.[2p] In addition, the reactivity of Ru-bda catalysts is particularly dependent on the axial ligands, and a minor change on the axial ligands could have dramatic influence on the reactivity of Ru-bda catalysts. For instance, one of the catalysts, [Ru(bda)-(isoq)$_2$] (**A**; isoq = isoquinoline), exhibits a turnover frequency of over 300 s^{-1} using Ce^{IV} as oxidant while [Ru(bda)(pic)$_2$] (**B**; pic = 4-picoline) shows only a TOF of 32 s^{-1} under the same reaction conditions.[7b] The increased TOF of the former isoquinoline-containing catalyst was due to the intermolecular $\pi-\pi$ stacking of the axial ligands, which facilitates the coupling of two Ru^{V}=O species in the O−O bond formation step. The second observation is from the comparison between [Ru(bda)-(dmso)(IMBr)] (**C**; dmso = dimethyl sulfoxide and IMBr = 5-bromo-N-methylimidazole) and [Ru(bda)(IMBr)$_2$] (**D**).[7d] The introduction of dmso leads to 40 fold increase in the reactivity in comparison with complex **D**. The third observation comes from [Ru(bda)(ptz)$_2$] (**E**; ptz = phthalazine).[7c] The major degradation of Ru-bda catalysts is the axial ligand dissociation. Replacing two isoquinoline ligands by two phthalazine ligands leads to conspicuous increase of the lifetime of **E** and its turnover number (55400 for **E** versus ca. 8400 for **A**). These observations motivated us to systematically study the axial ligand effects, for instance the electronic effect and the hydrophobic effect, with the view to improving their efficiency toward water oxidation. In aqueous solutions, the hydrophobic effect will help to bring molecules together and thereby favors the second order reactions, for instance the O−O bond formation of the Ru-bda catalysts. Herein, we report the synthesis and characterization of a series of mononuclear Ru complexes Ru(bda)L_2 (L = [$HNEt_3$][3-SO_3-pyridine], **1**; 4-(EtOOC)-pyridine, **2**; 4-bromopyridine, **3**; pyridine, **4**; 4-methoxypyridine, **5**; 4-(Me_2N)-pyridine, **6**; 4-[$Ph(CH_2)_3$]-pyridine, **7**; Figure 2), employ their electrochemistry in aqueous solutions, examine their catalytic activities toward Ce^{IV}-driven water oxidation, and reveal the structure−activity relationship of the Ru-bda family.

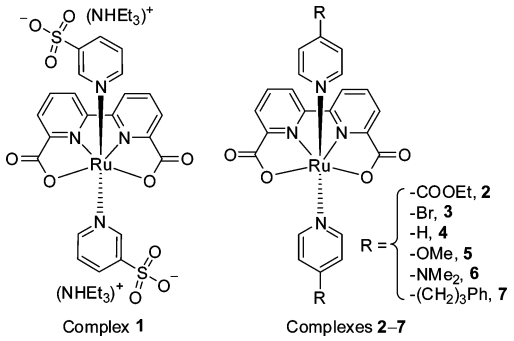

Figure 2. Molecular structures of complexes **1**−**7**.

SYNTHESIS AND CHARACTERIZATION

Complexes **1**−**7** were synthesized by procedures similar to those used for complexes **A** and **B**.[7b] Complexation of *cis*-[Ru(dmso)$_4$Cl$_2$] and H_2bda in the presence of triethylamine, followed by adding excess of the free axial ligands, yielded the corresponding mononuclear Ru-bda catalysts **1**−**7**. All of the complexes were characterized by ^{1}H NMR, high resolution mass spectrometry, and elemental analysis. Because of the strong electron donating ability of bda^{2-}, these Ru^{II} complexes could be oxidized to their Ru^{III} forms by molecular oxygen in solution, which leads to a problem in obtaining sharp signals in ^{1}H NMR spectra. However, this problem could be solved by adding a small amount of ascorbic acid as a reductant to the NMR samples. The C_{2v} symmetry of these complexes reduces the complexity of each ^{1}H NMR spectrum. Take complex **3** for instance (Figure 3). Three peaks at 8.51 (dd, 2H), 8.05 (dd, 2H), and 7.88 (t, 2H) ppm represent the proton resonances of bda^{2-}; two doublets at 7.64 (d, 4H) and 7.37 (d, 4H) ppm are assigned to the aromatic protons of two 4-Br-pyridine ligands.

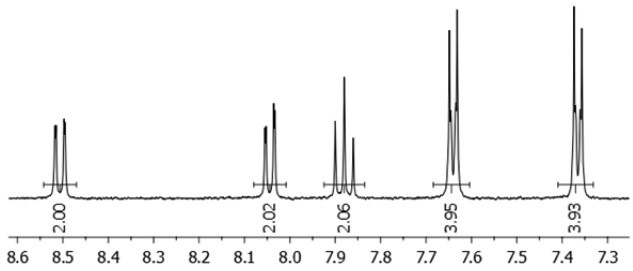

Figure 3. ^{1}H NMR spectrum (400 MHz, methanol-d_4 + dichloro-methane-d_2 with a small amount of ascorbic acid) of complex **3**.

Acetonitrile reacts readily with [Ru(bda)(pic)$_2$] in aqueous solutions. Complex **B** in either methanol-d_4 or D_2O/acetone-d_6 (9:1 v/v) remains its C_{2v} symmetry according to the ^{1}H NMR spectra (Figure 4). When D_2O/CD_3CN (9:1 v/v) was used as solvents, four broad proton resonance peaks of bda^{2-} were observed with a ratio of 1:1:3:1, implicating the break of C_{2v}

dx.doi.org/10.1021/ic302687d | Inorg. Chem. 2013, 52, 7844−7852

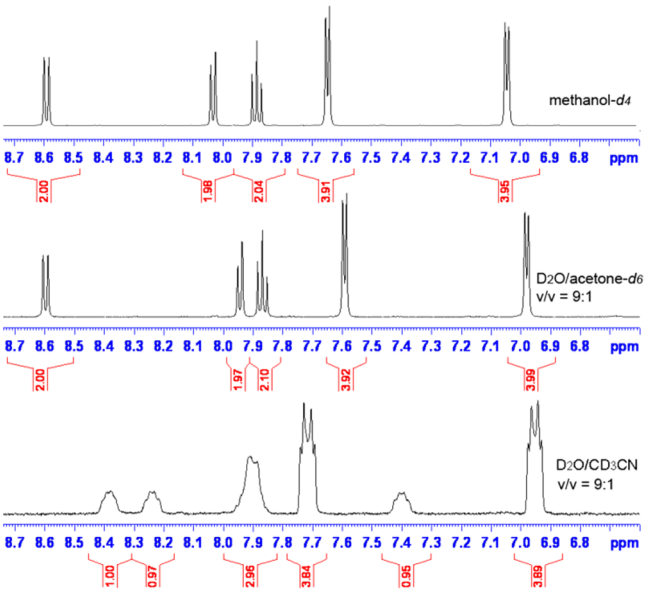

Figure 4. ^{1}H NMR spectra (500 MHz) of complex **B** in different solutions: (top) methanol-d_4, (middle) D_2O/acetone-d_6 (9:1 v/v), and (bottom) D_2O/CD_3CN (9:1 v/v).

symmetry (Figure 4, bottom). We propose that the resulting product is six-coordinate [Ru($\kappa_3^{O,N,N}$-bda)(pic)$_2$(MeCN)], one carboxylate dissociating from the Ru center (Figure 5, top).

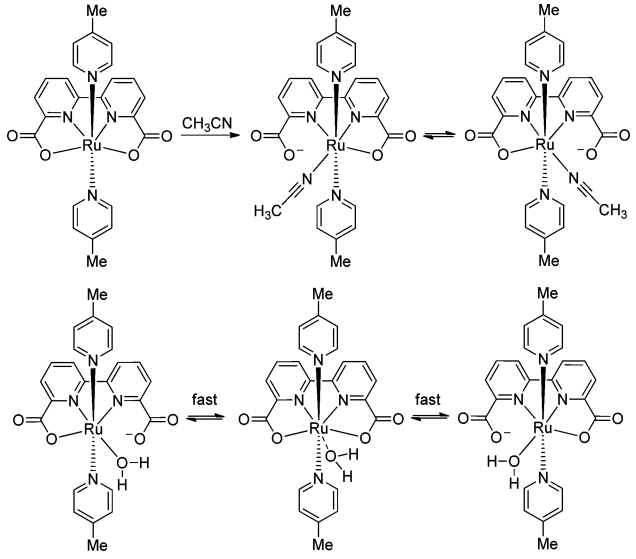

Figure 5. Schematic illustration of the reactions between complex **B** and solvents (top: acetonitrile; bottom: water).

Accordingly, the coordination between carboxylate and ruthenium(II) is weak. The slow structural exchange of the resulting complex makes the proton resonance peaks of bda^{2-} broad (Figure 4, bottom).

Previous study on the Pourbaix diagram of complex **B** suggests that dissolution of complex **B** in aqueous solutions yields a Ru-bda aqua complex.[7b] Unfortunately, this Ru aqua species could not be captured by the mass spectrometer, and only the [M + H]$^+$ species was observed, implying weak coordination between the aqua ligand and the ruthenium(II) cation. Considering the weak coordination between carboxylate and Ru^{II}, we propose the aqua complex as [Ru($\kappa_3^{O,N,N}$-bda)(pic)$_2$(OH$_2$)] (named as Ru^{II}–OH$_2$). The sharp proton resonance peaks of complex **B** in the mixed D_2O/acetone-d_6 (Figure 4, middle) indicate the fast structural exchange (Figure 5, bottom). However, we could not exclude the possibility that the Ru^{II}–OH$_2$ species is seven coordinated. Further investigation of the coordination sphere of Ru^{II}-bda complexes is in progress. Nevertheless, oxidation of **B** to higher valent states leads to stronger binding of carboxylate to the Ru cation and the formation of seven-coordinate Ru species, as evidenced by the isolation of the seven-coordinate Ru^{IV} species of **B**. It is well-known that the carboxylate is a "hard" ligand and binds more strongly to the high valent Ru cations than to the low oxidation state Ru cations. Thereby, the formation of seven-coordinate Ru^{IV} species in a $\kappa_4^{O,O,N,N}$-bda fashion is reasonable although the binding between the Ru^{II} cation and carboxylate is weak.

The crystal structures of complexes **1** and **6** have been resolved and are depicted in Figure 6. The selected bond

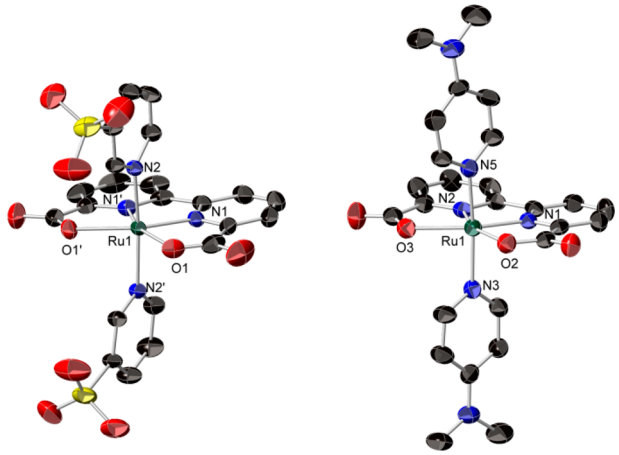

Figure 6. X-ray crystal structures of complexes **1** (left) and **6** (right) with thermal ellipsoids at 50% probability (hydrogen atoms, solvated MeOH molecules, and counterions are omitted for clarity).

Table 1. Selected Bond Lengths [Å] and Angles [deg] for Complexes 1 and 6

Complex **1**		Complex **6**	
N1–Ru1	1.923(3)	N1–Ru1	1.923(4)
N1′–Ru1	1.923(3)	N2–Ru1	1.915(4)
N2–Ru1	2.080(2)	N3–Ru1	2.095(4)
N2′–Ru1	2.080(2)	N5–Ru1	2.087(4)
O1–Ru1	2.185(3)	O2–Ru1	2.188(4)
O1′–Ru1	2.185(3)	O3–Ru1	2.196(4)
N1–Ru1–O1	78.3(1)	N1–Ru1–O2	77.72(16)
N1–Ru1–N1′	82.1(1)	N2–Ru1–N1	82.16(18)
N1′–Ru1–O1′	78.3(1)	N2–Ru1–O3	77.99(16)
O1–Ru1–O1′	121.39(9)	O2–Ru1–O3	122.12(13)

lengths and angles are listed in Table 1. The Ru–N bonds fall in the range of 1.915–2.095 Å; equatorial Ru–N bonds are slightly shorter than the axial ones. The octahedral coordination configuration of Ru atom is strongly distorted with the O1–Ru1–O1′ angle of 121.39° for **1** and the corresponding O2–Ru1–O3 angle of 122.12° for **6**, which is similar to the previously reported configuration of complex **B** (O2–Ru1–O3

dx.doi.org/10.1021/ic302687d | Inorg. Chem. 2013, 52, 7844–7852

angle, 122.99°).[7a] These angles are significantly larger than the O−Ru−O angle (90°) in an ideal octahedron, which plays a critical role for this type of catalysts to form seven-coordinate Ru intermediates with water molecules.

ELECTROCHEMISTRY

The potential/pH diagram (Pourbaix diagram) of complex **B** has been studied previously and revealed the proton transfer sequence of **B** at pH 1 upon oxidation as follows: $Ru^{II}-OH_2 \rightarrow Ru^{III}-OH_2 \rightarrow Ru^{IV}-OH \rightarrow Ru^{V}=O$.[7b] Herein, complex **1** bearing two sulfonate substitutes is water-soluble and is a good candidate for studying its potential change versus pH in aqueous solutions. Its Pourbaix diagram is shown in Figure 7.

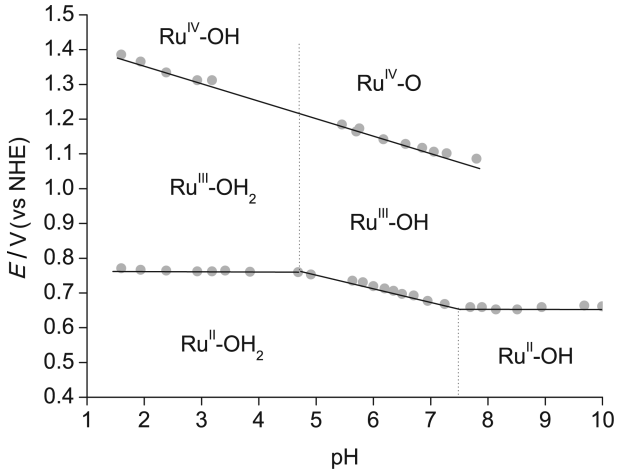

Figure 7. Pourbaix diagram of complex **1**. The potential values were obtained from its differential pulse voltammograms at various pH (Supporting Information, Figure S1). Working electrode: pyrolytic grahite electrode (basal plane). The $Ru^{IV/III}$ peaks are broad shoulder peaks in the differential pulse voltammograms and thereby the error of the estimated $E(Ru^{IV/III})$ values are large.

The oxidation of $Ru^{II}-OH_2$ involves only electron transfer at pH < 4.8 and becomes proton-coupled at 4.8 < pH < 7.5 (slope ≈ 45 mV per pH unit). At pH > 7.5, deprotonation of $Ru^{II}-OH_2$ occurs, generating $Ru^{II}-OH$, the oxidation of which gives $Ru^{III}-OH$ without proton transfer. The pK_a values of $Ru^{II}-OH_2$ and $Ru^{III}-OH_2$ are 7.5 and 4.8, respectively. The oxidation of $Ru^{III}-OH_2$ and $Ru^{III}-OH$ is coupled with one proton transfer (slope ≈ 50 mV per pH unit). The peak of $Ru^{V/IV}$ could not be assigned clearly because of the overlap of this peak with the catalytic peak. The Pourbaix diagram of **1** is in good agreement with the early observation about complex **B**. Considering the structural similarity of complexes **1**−**7** and **B**, we assume that the redox processes observed at pH 1.0 conditions correspond to $Ru^{II}-OH_2 \rightarrow Ru^{III}-OH_2 \rightarrow Ru^{IV}-OH \rightarrow Ru^{V}=O$ for all of these Ru-bda complexes.

Since not all of complexes **1**−**7** are water-soluble, CF_3CH_2OH was used to increase the solubility of complexes **2**−**7** in the aqueous electrolytes. The introduction of CF_3CH_2OH brought two issues to the electrochemistry measurements: (i) are the Ru-bda complexes stable in the present of CF_3CH_2OH? (ii) can CF_3CH_2OH be oxidized by a high energy electrode, for example electrode at 1.6 V, or by electrochemically generated Ru oxo species?

First, we tried to address the first issue by monitoring the UV−vis spectral change of complex **1** in an aqueous solution upon addition of CF_3CH_2OH (Supporting Information, Figure S2). Complex **1** in the pH 1.0 aqueous solution has a maximum MLCT (metal-to-ligand charge-transfer) absorption at 376 nm. This band was shifted to 370 nm in the mixed pH 1.0/CF_3CH_2OH (5:1 v/v) aqueous solution. This small change did not reflect a big structural change of complex **1**. Next, proton NMR spectra of complex **1** in various concentrations of CF_3CD_2OD aqueous solutions were recorded (Supporting Information, Figure S3). Two peaks were shifted obviously upon addition of CF_3CD_2OD. However, no decomposition of complex **1** was observed: (i) the C_{2v} symmetry was not broken, and (ii) no axial ligand dissociation occurred. Unfortunately, it is not clear whether the spectral change in both UV−vis and NMR spectra is due to the solvation effect or the coordination of CF_3CH_2OH to the Ru cation.

The oxidation of CF_3CH_2OH was examined by means of electrochemistry. The cyclic voltammograms of complex **2** in aqueous pH 1.0 solutions with various concentration of CF_3CH_2OH were recorded and depicted in Supporting Information, Figure S4. If CF_3CH_2OH can be easily oxidized by Ru=O species of our catalyst **2** or the electrode, addition of CF_3CH_2OH in the aqueous solution of complex **2** will result in the growth of the catalytic current. As shown in Supporting Information, Figure S4, addition of CF_3CH_2OH did not lead to increase of the catalytic current, suggesting that negligible oxidation of CF_3CH_2OH, if any, occurs. Contrarily, the current decreases upon addition of CF_3CH_2OH, showing the inhibiting ability of CF_3CH_2OH toward water oxidation.

Figure 8 (top) representatively depicts the cyclic voltammogram (CV) and the differential pulse voltammogram (DPV) of

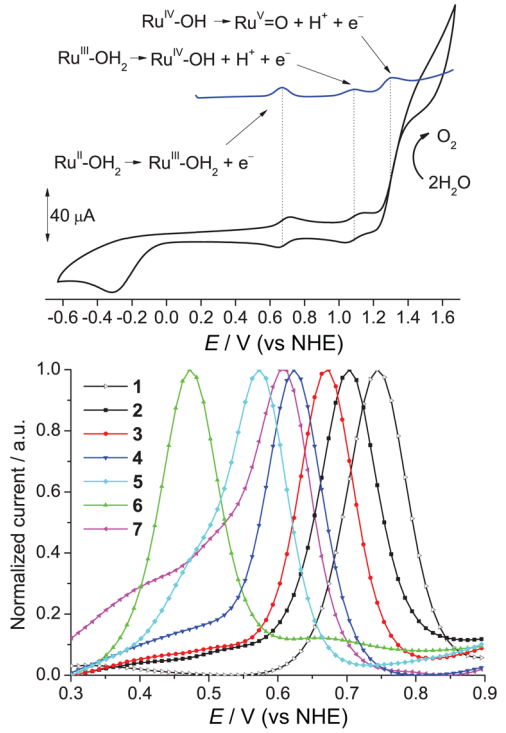

Figure 8. Top: the CV (black) and DPV (blue) of complex **3**. Bottom: normalized DPVs of complexes **1**−**7**. Conditions: **1**−**6** in the mixed CF_3CH_2OH/pH 1.0 aqueous solution (1:2 v/v); **7** in the mixed CF_3CH_2OH/pH 1.0 aqueous solution (2:1 v/v). Oxidation peak at 0.4 V in the DPV of **7** is attributed to the impurity of the electrolyte (see more in Supporting Information, Figure S5).

dx.doi.org/10.1021/ic302687d | Inorg. Chem. 2013, 52, 7844−7852

complex **3**. At the range 0.2−1.6 V, three redox waves were observed at 0.67 V, 1.09 V, and 1.30 V, corresponding to Ru^{III}−OH_2/Ru^{II}−OH_2, Ru^{IV}−OH/Ru^{III}−OH_2, and Ru^{V}=O/Ru^{IV}−OH processes, respectively. A catalytic current started arising after Ru^{V} was generated, implying Ru^{V} triggers water oxidation. From the cathodic scan, a reduction peak at about −0.3 V was observed, corresponding to the reduction of molecular O_2 generated electrochemically from the anodic scan. Owing to the strong electron-donating ability of bda^{2-}, the oxidation potentials of **3**, especially for the oxidation steps only involving electron transfer,[2q] are significantly lower than those of other Ru water oxidation catalysts with neutral ancillary ligands. For instance, under pH 1.0 conditions, the well-studied $[Ru(tpy)(bpy)(OH_2)]^{2+}$ (tpy = 2,2′:6′,2″-terpyridine; bpy = 2,2′-bipyridine) complex exhibits three oxidation waves at 1.04 V for Ru^{III}−OH_2/Ru^{II}−OH_2, 1.23 V for Ru^{IV}=O/Ru^{III}−OH_2, and 1.80 V for Ru^{V}=O/Ru^{IV}=O,[2b], and Meyer's $[Ru(tpy)(bpm)(OH_2)]^{2+}$ (bpm = 2,2′-bipyrimidine) complex shows a two-electron Ru^{II}−OH_2/Ru^{IV}=O wave at about 1.18 V and a Ru^{V}=O/Ru^{IV}=O wave at 1.65 V.[2i] Besides Ru-bda aqua complexes, many other transition metal complexes carrying negatively charged ligands (R-COO^-, Ph-O^-, RR′N^-, and HO^-/O^{2-}) possess low oxidation potentials, and their high oxidation states are stabilized dramatically. For example, the blue dimer **F**, *trans*-oxoaquoruthenium(IV) complex **G** ($E_{1/2}$($Ru^{IV/III}$) = 0.86 V vs NHE (0.62 vs SCE)) and mononuclear Mn^{V}-oxo complex **H** are of the representative complexes (Figure 9).[8] Stabilization of the high valent metal

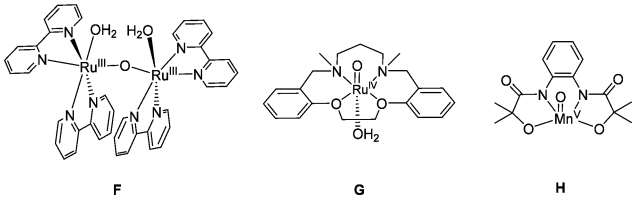

Figure 9. Molecular structures of complexes **F**−**H**.

oxo species eventually could reduce the oxidative damage of the ancillary ligands of metal complexes while it would decrease the oxidizing power of the metal oxo species and the reactivity toward oxidation reactions.

Figure 8 (bottom) shows the normalized DPVs of complexes **1**−**7** in the mixed CF_3CH_2OH/pH 1.0 aqueous solutions (only $Ru^{III/II}$ peaks are shown). The potentials of $E_{1/2}$(Ru^{III}−OH_2/Ru^{II}−OH_2) of these complexes are apparently dependent on the nature of axial pyridine ligands. As expected, $E_{1/2}$(Ru^{III}−OH_2/Ru^{II}−OH_2), spanning from 0.47 to 0.75 V, decreases when the axial ligand is varied from the electron withdrawing one to the electron donating one. The difference in $E_{1/2}$(Ru^{IV}−OH/Ru^{III}−OH_2) of these complexes is within 50 mV with an exception of complex **1** (not shown herein); the onset potentials of catalytic curves are close to each other. Apparently, the electronic effect is less pronounced on the higher Ru oxidation states (+IV and +V) of Ru-bda complexes.

The linear potential sweep voltammograms of complexes **1**−**6** in the mixed CF_3CH_2OH/pH 1.0 (1:2 v/v) solutions are represented in Figure 10 (complex **7** is poorly soluble in above mixed solvent). It was observed that complexes **2** and **3** with electron deficient axial ligands gave higher catalytic current in comparison with complexes **4**, **5**, and **6** with electron rich ligands. However, the most electron deficient complex **1** raised

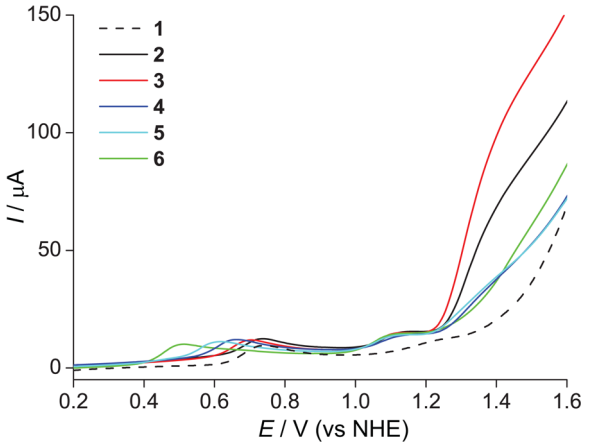

Figure 10. Linear potential sweep voltammograms (*i*-*E* curves) of complexes **1**−**6** in the mixed CF_3CH_2OH/pH 1.0 aqueous solution (1:2 v/v).

the lowest catalytic current. Two reasons may cause the low efficiency of **1**. (i) The hydrophilic effect of the sulfonate substituted axial ligand reduces the entropy contribution to the O−O bond coupling step in comparison with other hydrophobic axial ligands. Note that the hydrophobic/hydrophilic effects originate from the disruption of hydrogen bonding of water molecules by the solute. To minimize the surface tension of water molecules surrounding the nonpolar solute molecules, the solute molecules tend to get together and minimize the surface area exposing to water. This is so-called hydrophobic effect, which is mainly controlled by the entropy change. The hydrophilic effect has an opposite effect. (ii) The stereo-repulsion raised by sulfonate groups might slow down the coupling step. Generally, the electron-withdrawing groups have positive effect on the electrochemical water oxidation activity. This is probably because electron deficient substitutes thermodynamically destabilize the Ru^{V}=O (or the cationic radical Ru^{IV}−$O^{\bullet}$ species), make the oxo species more reactive, and eventually enhance the O−O bond formation. The trend of electronic effect also reflects that the electron density of the Ru center is developing from Ru^{V}=O to the transition state (Ru^{V}−O···O−Ru^{V}) of the rate determining step.

To dissolve complex **7** and test its electrochemical catalytic activity, we increased the ratio of CF_3CH_2OH/pH 1.0 to 2/1 (v/v). The CV of complex **7** together with that of **B** are depicted in Figure 11. Note that the C−H (py−CH_2−) bond of complex **7** is stable against electrochemical oxidation under the given conditions (Supporting Information, Figure S6). Complex **B** in pH 1/CF_3CH_2OH (1:2 v/v) showed a smaller catalytic current than its pH 1/CF_3CH_2OH (2:1 v/v) solution.[7b] The decrease of the catalytic current most likely is caused by the coordination of CF_3CH_2OH, which inhibits the access of water to the catalyst. Coordination of CF_3CH_2OH to Meyer's Ru catalyst has been documented.[9] Nevertheless, under the same conditions pH 1/CF_3CH_2OH (1:2 v/v), complex **7** shows a better electrochemical catalytic activity than complex **B**. Since complexes **7** and **B** have almost identical E($Ru^{III/II}$), the electronic effect could be ruled out as the major contribution to the activity difference. We believe that this is due to the influence of hydrophobic chains of complex **7**, which contributes to the entropy change and facilitates the radical coupling step (2 Ru^{V}=O → Ru^{IV}−O−O−Ru^{IV}) when two molecules couple to each other in the aqueous solution.

dx.doi.org/10.1021/ic302687d | *Inorg. Chem.* 2013, 52, 7844−7852

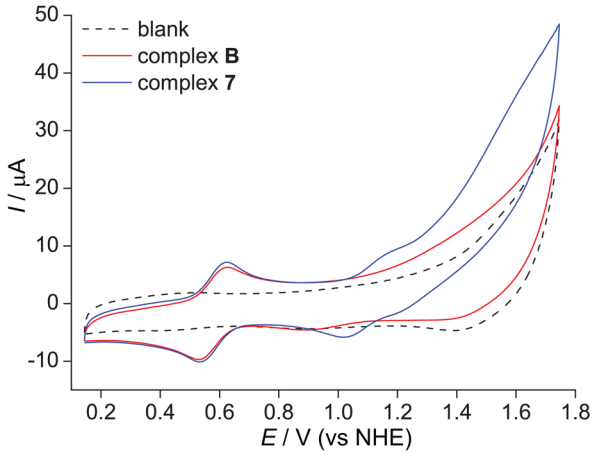

Figure 11. CVs of complexes **7** and **B** in the mixed CF_3CH_2OH/pH 1.0 aqueous solution (2:1 v/v).

WATER OXIDATION

As is known, water oxidation is favored at high pH conditions while proton reduction to dihydrogen is favored at low pH conditions. To promote the hydrogen production, it becomes interesting to consider the catalytic activity of water oxidation catalysts under acidic environments. Commonly, Ce^{IV} is a widely used as a sacrificial electron acceptor in homogeneous water oxidation study although it has to be conducted at low pH solutions, usually pH 1.0, which is too much for practical application. For convenience, we still use Ce^{IV} as oxidant in pH 1.0 to evaluate the catalytic ability of complexes **1**−**7**. Generally, a catalyst in the mixed acetonitrile/pH 1.0 was injected in an acidic aqueous solution containing Ce^{IV}. Bubbles were observed immediately. The oxygen evolution was recorded by monitoring the pressure change of the gas phase. Although several groups have observed significant CO_2 production by using other water oxidation catalysts, the CO_2 production in our system is negligible. It is most likely because (i) the Ru^{V}═O species of our Ru-bda catalysts are much less oxidizing than other Ru water oxidation catalysts, as can be seen from the low redox potentials of $Ru^{V/IV}$, and (ii) the rapid O−O bond formation (2 Ru^{V}═O → Ru^{IV}−O−O−Ru^{IV}) suppresses the oxidative decomposition markedly. We thereby assume that the pressure change in our case is attributed to oxygen generation.

Since the oxygen evolution is second order in the concentrations of our catalysts, the high catalyst concentration [catalyst] favors the oxygen evolution. To obtain a high oxygen evolving rate, we chose high catalyst loading. The concentrations of catalysts and Ce^{IV} are respectively 2.16×10^{-4} M and 0.327 M ([catalyst]/[Ce^{IV}] ≈ 6.6/10000). The plots of oxygen evolution versus time were represented in Figure 12. The fastest two water oxidation catalysts are **2** and **3** with oxygen evolution rates being 119 and 115 mols of O_2 per mole of catalyst per second, respectively. Complexes **4**, **5**, and **6** rank in the middle with respective rates of 25, 25, and 14 mols of O_2 per mole of catalyst per second, then followed by complex **1** (9.8 mols of O_2 per mole of catalyst per second). Since the solubility of complex **7** is very poor in water, it precipitated out immediately when a solution of **7** was injected in the operating system. Thereby the rate obtained for **7** (4 mols of O_2 per mole of catalyst per second) is not comparable with others. According to the electronic effect observed in the electrochemistry study, it is reasonable that complexes with electron-withdrawing groups, such as **2** and **3**, exhibit better performances than those with electron-donating groups, such as **4**, **5**, and **6**. Complex **1** with two hydrophilic and bulk sulfonate groups showed a relatively low oxygen evolution rate, which is in agreement with its electrochemical catalytic activity.

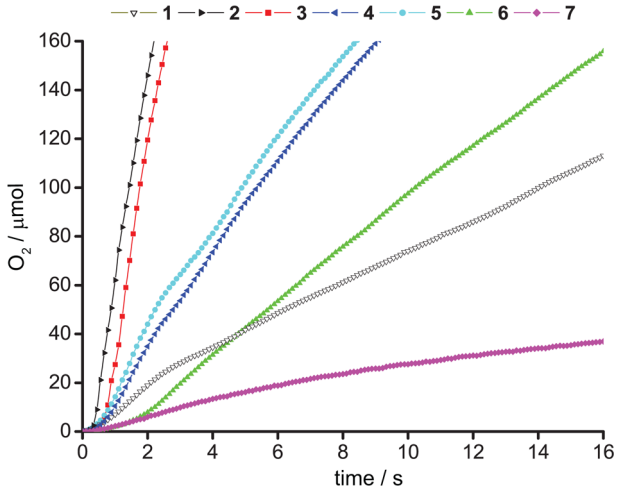

Figure 12. Plots of oxygen evolution versus time. Conditions: 3.6 mL of solution, catalyst (8×10^{-7} mol, 2.16×10^{-4} M) and Ce^{IV} (1.18×10^{-3} mol, 0.327 M).

Under above reaction conditions, Ce^{IV} was consumed totally within one minute, and thereby the turnover numbers are limited by the amount of Ce^{IV}. We thereby decreased the [catalyst] to evaluate their durability. In this case, the concentrations of catalysts and Ce^{IV} are respectively 1.20×10^{-5} M and 0.365 M ([catalyst]/[Ce^{IV}] ≈ 3.3/100000). The TONs are respectively 360 for **1**, 4800 for **2**, 4500 for **3**, 580 for **4**, 760 for **5**, and 790 for **6** (Figure 13). Because of the solubility issue, complex **7** was not examined.

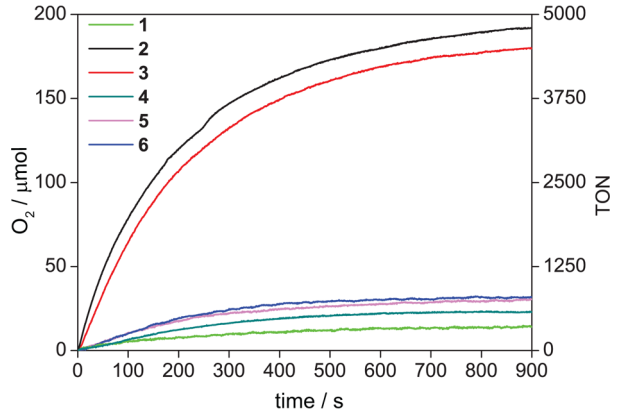

Figure 13. Plots of oxygen evolution versus time. Conditions: 3.22 mL of solution, catalyst (4×10^{-8} mol, 1.20×10^{-5} M) and Ce^{IV} (1.18×10^{-3} mol, 0.365 M).

Besides, we have found that strong noncovalent interactions display more prominent effects on the catalytic activity in comparison with the electronic effect. For example, complexes **4** and **A** (see ref 7b) have almost identical redox potentials of $Ru^{II/III}$ (E = 0.62 for **4** and 0.63 for **A**) but very distinct activity. Under the same conditions, complex **A** exhibits a TOF of 300 per second while complex **4** gives only 25 per second. It is proposed, in the early work, that the intermolecular π−π stacking of the axial isoquinoline ligands of complex **A**

dx.doi.org/10.1021/ic302687d | Inorg. Chem. 2013, 52, 7844−7852

promotes the O−O bond formation step and makes **A** far superior to **4**. We have also reported that strong binding of the axial ligand to the Ru center could result in a robust Ru-bda catalyst. In other words, strong electron donating ligands could enhance the longevity of Ru-bda catalysts. The electronic effect on the longevity is contrary to that on the reactivity. Of course, a good catalyst should have both high reactivity and longevity besides the low cost and the low overpotential. Then, how to solve this paradoxical effect? Our observation of the non-covalent interaction effect could solve it just because the noncovalent interactions are more effective than the electronic effect on the reactivity (**A** versus **4**). Thereby, to design a more robust and active Ru-bda catalyst requires the axial ligands more electronically rich and more "attractive" to each other.

CONCLUSIONS

A series of Ru-bda complexes **1**−**7** have been prepared, characterized, and examined as water oxidation catalysts under typical Ce^{IV}-driven water oxidation conditions. At the Ru^{II} state, the carboxylate (bda^{2-}) is labile while it binds to higher valent Ru cations more strongly. The Pourbaix diagram of complex **1** was obtained and revealed an oxidation sequence of $Ru^{II}-OH_2 \rightarrow Ru^{III}-OH_2 \rightarrow Ru^{IV}-OH \rightarrow Ru^{V}=O$ at pH 1.0, which is in agreement with the observations of complex **B**. In comparison with neutral ligands, such as bpy and tpy, the strong electron donating ability of bda^{2-} and HO^-/O^{2-} make the Ru-bda aqua complexes readily access high valent Ru states up till +V at relatively low potentials. The electronic effect on the water oxidation activity has been examined by installing different axial ligands: electron-withdrawing and -donating pyridyl ligands. Electron withdrawing groups enhance the catalytic activity of Ru-bda water oxidation catalysts while electron donating ones give negative effect. By comparison of complex **7** with complex **B**, it is concluded that the hydrophobic effect can enhance the activity of Ru-bda catalysts.

EXPERIMENTAL SECTION

General Procedures. 2,2′-Bipyridine-6,6′-dicarboxylic acid (H_2bda) was purchased from Jinan Henghua Sci. & Tec. Co. Ltd., and *cis*-[$Ru(dmso)_4Cl_2$] was prepared according to the literature method.[10] All other chemicals are commercially available. All solvents are reagent grade and predeoxygenated. The ^1H NMR spectra were recorded with either 400 or 500 MHz of Bruker Avance spectrometer. High resolution mass spectrometry (HR-MS) measurements were performed on a Q-Tof Micro mass spectrometry. Elemental analyses were performed with a Thermoquest-Flash EA 1112 apparatus. Cyclic voltammetric (CV) measurements were carried out with either Autolab potentiostat with a GPES electrochemical interface (Eco Chemie), with pyrolytic graphite electrode (either basal or edge plane) as working electrodes, Pt wire as auxiliary, and measured versus SCE reference electrode. The scan rate is 0.1 V/s. All potentials reported here are converted to their corresponding value versus NHE, using an internal reference $[Ru(bpy)_3]^{2+}$ ($E_{1/2}(Ru^{III/II})$ = 1.26 V versus NHE).

The oxygen evolution was recorded with a pressure transducer (Omega PX138−030A5 V) driven at 8.00 V using a power supply (TTi-PL601) plus a data acquisition module (Omega OMB-DAQ-2416; running at 8 Hz for our measurements) and the final amount of oxygen was calibrated by GC (GC-2014 Shimadzu; equipped with a thermal conductive detector, a 5 Å molecular sieve column and with He as carrier gas) in a separate experiment. The pressure transducer was calibrated by injecting a certain amount of gas, and the response of the transducer is fast and the data is reproducible. Note: for curves related to complexes **1**, **4**, **5**, and **6** in Figure 13, the final amount of oxygen was not calibrated by GC. The general procedures about oxygen measurements were reported previously.[7b]

Complex 1. A mixture of 2,2′-bipyridine-6,6′-dicarboxylic acid (H_2bda) (100 mg, 0.41 mmol), *cis*-[$Ru(dmso)_4Cl_2$] (200 mg, 0.41 mmol), and NEt_3 (0.8 mL) in methanol (30 mL) was degassed with N_2 and refluxed over 3 h. An excess of 3-pyridyl sulfonic acid (0.52 g, 3.27 mmol) was added and the mixture was heated to reflux overnight. The solvent was removed, and the solid was redissolved in about 2 mL of methanol, which was then placed in the fume hood stationarily over two weeks. Crystals were filtered out, washed with the mixed MeOH/Et_2O (1:1 v/v), and dried under vacuum. Complex **1**·2MeOH was obtained as dark crystals (110 mg, yield: 31%). More crystals could be obtained from the filtrate by recrystallization over weeks. ^1H NMR (500 MHz, D_2O with a small amount of (+)-sodium L-ascorbate): δ = 8.57 (d, 2H), 8.20 (d, 2H), 8.01−7.93 (m, 8H), 7.35 (t, 2H), 3.16 (q, 12H), 1.23 (t, 18H). HRMS (ESI): m/z^+ = 682.9103 ($M + Na^+$), calcd: 682.9098; Found: C 46.21, H 5.79, N 9.15. Calc. For $C_{34}H_{46}N_6O_{10}RuS_2 \cdot 2CH_3OH$: C 46.59, H 5.86, N 9.06%.

Procedures similar to those described for **1** were followed using 4-substituted pyridines instead of 3-pyridyl sulfonic acid to afford the corresponding complexes **2**−**7** (*ethanol was used instead of methanol for complex* **2** *to avoid transesterification*). For these complexes, the purification was conducted by column chromatography on silica gel using gradient eluents (dichloromethane-methanol).

Complex 2. Yield: 57%. ^1H NMR (500 MHz, methanol-d_4 + $CDCl_3$ with a small amount of (+)-sodium L-ascorbate): δ = 8.60 (d, 2H), 8.06−8.03 (m, 6H), 7.93 (t, 2H), 7.68 (d, 4H), 4.33 (q, 4H), 1.32 (t, 6H). HRMS (ESI): m/z^+ = 646.0632 (M^+), calcd: 646.0638; Found: C 51.85, H 3.75, N 8.62. Calc. For $C_{28}H_{24}N_4O_8Ru$: C 52.09, H 3.75, N 8.68%.

Complex 3. Yield: 24%. ^1H NMR (400 MHz, methanol-d_4 + dichloromethane-d_2 with a small amount of ascorbic acid): δ = 8.51 (d, 2H), 8.05 (d, 2H), 7.88 (t, 2H), 7.64 (d, 4H), 7.37 (d, 4H). HRMS (ESI): m/z^+ = 660.8518 ($M + H^+$), calcd: 660.8486; Found: C 38.59, H 2.40, N 7.85. Calc. For $C_{22}H_{14}Br_2N_4O_4Ru \cdot 1.5H_2O$: C 38.50, H 2.50, N 8.16%.

Complex 4. Yield: 34%; ^1H NMR (400 MHz, methanol-d_4 + dichloromethane-d_2 with a small amount of ascorbic acid): δ = 8.57 (d, 2H), 8.04 (d, 2H), 7.88 (t, 2H), 7.83 (d, 4H), 7.65 (t, 2H), 7.18 (t, 4H); HRMS (ESI): m/z^+ = 503.0315 ($M + H^+$), calcd: 503.0294; Found: C 51.49, H 3.31, N 10.84. Calc. For $C_{22}H_{16}N_4O_4Ru \cdot 0.5H_2O$: C 51.76, H 3.36, N 10.98%.

Complex 5. Yield: 41%; ^1H NMR (400 MHz, methanol-d_4 + dichloromethane-d_2 with a small amount of ascorbic acid): δ = 8.48 (d, 2H), 8.03 (d, 2H), 7.82 (t, 2H), 7.55 (d, 4H), 6.71 (d, 4H), 3.76 (s, 6H); HRMS (ESI): m/z^+ = 5563.0543 ($M + H^+$), calcd: 563.0505; Found: C 48.91, H 3.52, N 9.26. Calc. For $C_{24}H_{20}N_4O_6Ru \cdot 1.3H_2O$: C 49.28, H 3.89, N 9.58%.

Complex 6. Yield: 27%; ^1H NMR (400 MHz, methanol-d_4 + dichloromethane-d_2 with a small amount of ascorbic acid): δ = 8.39 (d, 2H), 8.02 (d, 2H), 7.74 (t, 2H), 7.16 (d, 4H), 6.30 (d, 4H), 2.88 (s, 12H); HRMS (ESI): m/z^+ = 589.1174 ($M + H^+$), calcd: 589.1137; Found: C 50.31, H 4.75, N 13.99. Calc. For $C_{26}H_{26}N_6O_4Ru \cdot 1.6H_2O$: C 50.66, H 4.77, N 13.63%.

Complex 7. Yield: 51%. ^1H NMR (500 MHz, methanol-d_4 + $CDCl_3$ with a small amount of (+)-sodium L-ascorbate): δ = 8.54 (d, 2H), 8.03 (d, 2H), 7.85 (t, 2H), 7.63 (d, 4H), 7.18 (t, 4H), 7.08−7.06 (m, 6H), 6.98 (d, 4H), 2.56−2.51 (m, 8H), 1.85−1.79 (m, 4H). HRMS (ESI): m/z^+ = 761.1668 ($M + Na^+$), calcd: 761.1678; Found: C 62.90, H 5.21, N 6.95. Calc. For $C_{40}H_{36}N_4O_4Ru \cdot 1.5H_2O$: C 62.81, H 5.14, N 7.33%.

Single crystals of complex **1** were obtained by recrystallization of **1** in methanol. Single crystal X-ray diffraction data were collected on an Oxford Xcalibur 3 with molybdenum radiation (λ = 0.71073 Å). Data reduction and absorption correction were applied with CrysAlis. The structure (Table 2) was solved by SUPERFLIP[11] in the WinGX package.[12] Hydrogen atoms were located in the Fourier difference maps, except for those on the carbon atoms of the disordered $HNEt_3^+$ which were geometrically positioned on parent atoms using a riding model. All non-hydrogen atoms were refined with anisotropic displacement parameters with SHELXL97 using a full-matrix least-squares technique on F^2.[13] The data resolution for **1** was cut at 0.70 Å

dx.doi.org/10.1021/ic302687d | *Inorg. Chem.* 2013, 52, 7844−7852

Table 2. Summary of the Crystal Data for Complexes 1 and 6

	1	6
formula	$C_{36}H_{54}N_6O_{12}RuS_2$	$C_{26}H_{26}N_6O_4Ru$
formula weight	928.04	587.60
space group	$C2/c$ (No. 15)	$P\bar{1}$ (No. 2)
a/Å	21.2732(7)	8.211(4)
b/Å	8.1023(2)	11.037(8)
c/Å	26.1598(5)	15.89(2)
α/deg	90.00	70.23(8)
β/deg	112.677(2)	78.96(6)
γ/deg	90.00	77.86(5)
V/Å^3	4160	1314
Z	4	2
D_c/g cm^{-3}	1.482	1.486
T/K	293	299
$F(000)$	1936	600
μ(MoKR)/mm^{-1}	0.71073	0.71073
refl. collected	6141	4581
goodness-of-fit on F^2	1.09	1.04
R_1 [$I > 2\sigma(I)$] (all)	0.057	0.078
wR_2 [$I > 2\sigma(I)$] (all)	0.126	0.119

because of weak reflections at higher 2θ values. CheckCIF on complex **1** raises one level A alert. This is due to the large difference in thermal parameters for hydrogen atoms. This is expected as the complex is well ordered and thus hydrogen atoms of the complex have low thermal parameters, while hydrogen atoms on the $HNEt_3$ cations have large thermal parameters. The large thermal parameters occur as the carbon atoms are disordered on $HNEt_3$ cations. As a riding model was used for hydrogen atoms on $HNEt_3$ cations, these hydrogen atoms have relatively larger thermal parameters. All other hydrogen atoms were ordered and were located in Fourier difference maps.

Single crystals of complex **6** were obtained by diffusion of an ether layer on the top of a methanolic **6** solution. Single crystal X-ray diffraction data were collected on a Bruker-Nonius KappaCCD with molybdenum radiation (λ = 0.71073 Å). Data reduction was done with EvalCCD and absorption correction with SADABS. The structure was solved by Direct Methods (SHELXS97). Hydrogen atoms were placed at calculated positions and refined using a riding model. All non-hydrogen atoms were refined with anisotropic displacement parameters with SHELXL97 using a full-matrix least-squares technique on F^2.

■ ASSOCIATED CONTENT

Supporting Information

Differential pulse voltammograms (DPVs), UV−vis, and ^{1}H NMR spectra of complex **1** (Figure S1−S3), cyclic voltammograms of complex **2** under various [CF_3CH_2OH] (Figure S4), and DPVs of complex **7** (Figure S5). This material is available free of charge via the Internet at http://pubs.acs.org.

■ AUTHOR INFORMATION

Corresponding Author

*E-mail: lichengs@kth.se.

Author Contributions

The manuscript was written through contributions of all authors. All authors have given approval to the final version of the manuscript.

Notes

The authors declare no competing financial interest.

■ ACKNOWLEDGMENTS

This work is supported by the Swedish Research Council, the Knut & Alice Wallenberg Foundation, the Swedish Energy Agency, China Scholarship Council (CSC), the Basic Research Program of China (2009CB220009), and the National Natural Science Foundation of China (21120102036, 91233201).

■ REFERENCES

(1) (a) McDaniel, N. D.; Coughlin, F. J.; Tinker, L. L.; Bernhard, S. *J. Am. Chem. Soc.* **2008**, *130*, 210. (b) Hull, J. F.; Balcells, D.; Blakemore, J. D.; Incarvito, C. D.; Eisenstein, O.; Brudvig, G. W.; Crabtree, R. H. *J. Am. Chem. Soc.* **2009**, *131*, 8730. (c) Lalrempuia, R.; McDaniel, N. D.; Müller-Bunz, H.; Bernhard, S.; Albrecht, M. *Angew. Chem., Int. Ed.* **2010**, *49*, 9765. (d) Joya, K.; Subbaiyan, N.; D'Souza, F.; de Groot, H. *Angew. Chem., Int. Ed.* **2012**, *51*, 9601. (e) Petronilho, A.; Rahman, M.; Woods, J. A.; Al-Sayyed, H.; Muller-Bunz, H.; Don MacElroy, J. M.; Bernhard, S.; Albrecht, M. *Dalton Trans.* **2012**, *41*, 13074. (f) Schley, N.; Blakemore, J.; Subbaiyan, N.; Incarvito, C.; D'Souza, F.; Crabtree, R.; Brudvig, G. *J. Am. Chem. Soc.* **2011**, *133*, 10473. (g) Blakemore, J. D.; Schley, N. D.; Olack, G. W.; Incarvito, C. D.; Brudvig, G. W.; Crabtree, R. H. *Chem. Sci.* **2011**, *2*, 94. (h) Blakemore, J.; Schley, N.; Balcells, D.; Hull, J.; Olack, G.; Incarvito, C.; Eisenstein, O.; Brudvig, G.; Crabtree, R. *J. Am. Chem. Soc.* **2010**, *132*, 16017.

(2) (a) Wasylenko, D. J.; Ganesamoorthy, C.; Koivisto, B. D.; Berlinguette, C. P. *Eur. J. Inorg. Chem.* **2010**, 3135. (b) Wasylenko, D. J.; Ganesamoorthy, C.; Henderson, M. A.; Koivisto, B. D.; Osthoff, H. D.; Berlinguette, C. P. *J. Am. Chem. Soc.* **2010**, *132*, 16094. (c) Wada, T.; Tsuge, K.; Tanaka, K. *Angew. Chem., Int. Ed.* **2000**, *39*, 1479. (d) Muckerman, J. T.; Polyansky, D. E.; Wada, T.; Tanaka, K.; Fujita, E. *Inorg. Chem.* **2008**, *47*, 1787. (e) Xu, Y.; Åkermark, T.; Gyollai, V.; Zou, D.; Eriksson, L.; Duan, L.; Zhang, R.; Åkermark, B.; Sun, L. *Inorg. Chem.* **2009**, *48*, 2717. (f) Chen, Z.; Concepcion, J. J.; Meyer, T. J. *Dalton Trans.* **2011**, *40*, 3789. (g) Concepcion, J. J.; Tsai, M.-K.; Muckerman, J. T.; Meyer, T. J. *J. Am. Chem. Soc.* **2010**, *132*, 1545. (h) Concepcion, J. J.; Jurss, J. W.; Brennaman, M. K.; Hoertz, P. G.; Patrocinio, A. O. T.; Murakami Iha, N. Y.; Templeton, J. L.; Meyer, T. J. *Acc. Chem. Res.* **2009**, *42*, 1954. (i) Concepcion, J. J.; Jurss, J. W.; Templeton, J. L.; Meyer, T. J. *J. Am. Chem. Soc.* **2008**, *130*, 16462. (j) Romain, S.; Vigara, L.; Llobet, A. *Acc. Chem. Res.* **2009**, *42*, 1944. (k) Mola, J.; Dinoi, C.; Sala, X.; Rodríguez, M.; Romero, I.; Parella, T.; Fontrodona, X.; Llobet, A. *Dalton Trans.* **2011**, *40*, 3640. (l) Maji, S.; Vigara, L.; Cottone, F.; Bozoglian, F.; Benet-Buchholz, J.; Llobet, A. *Angew. Chem., Int. Ed.* **2012**, *51*, 5967. (m) Bernet, L.; Lalrempuia, R.; Ghattas, W.; Mueller-Bunz, H.; Vigara, L.; Llobet, A.; Albrecht, M. *Chem. Commun.* **2011**, *47*, 8058. (n) Duan, L.; Tong, L.; Xu, Y.; Sun, L. *Energy Environ. Sci.* **2011**, *4*, 3296. (o) An, J.; Duan, L.; Sun, L. *Faraday Discuss.* **2012**, *155*, 267. (p) Tong, L.; Duan, L.; Xu, Y.; Privalov, T.; Sun, L. *Angew. Chem., Int. Ed.* **2011**, *50*, 445. (q) Tong, L.; Wang, Y.; Duan, L.; Xu, Y.; Cheng, X.; Fischer, A.; Ahlquist, M. S. G.; Sun, L. *Inorg. Chem.* **2012**, *51*, 3388. (r) Tong, L.; Göthelid, M.; Sun, L. *Chem. Commun.* **2012**, *48*, 10025. (s) Kaveevivitchai, N.; Chitta, R.; Zong, R.; El Ojaimi, M.; Thummel, R. P. *J. Am. Chem. Soc.* **2012**, *134*, 10721. (t) Kaveevivitchai, N.; Zong, R.; Tseng, H.-W.; Chitta, R.; Thummel, R. P. *Inorg. Chem.* **2012**, *51*, 2930. (u) Polyansky, D. E.; Muckerman, J. T.; Rochford, J.; Zong, R.; Thummel, R. P.; Fujita, E. *J. Am. Chem. Soc.* **2011**, *133*, 14649. (v) Boyer, J. L.; Polyansky, D. E.; Szalda, D. J.; Zong, R.; Thummel, R. P.; Fujita, E. *Angew. Chem., Int. Ed.* **2011**, *50*, 12600. (w) Yoshida, M.; Masaoka, S.; Abe, J.; Sakai, K. *Chem.—Asian. J.* **2010**, *5*, 2369. (x) Yoshida, M.; Masaoka, S.; Sakai, K. *Chem. Lett.* **2009**, *38*, 702. (y) Masaoka, S.; Sakai, K. *Chem. Lett.* **2009**, *38*, 182. (z) Yagi, M.; Tajima, S.; Komi, M.; Yamazaki, H. *Dalton Trans.* **2011**, *40*, 3802. (aa) Yamazaki, H.; Hakamata, T.; Komi, M.; Yagi, M. *J. Am. Chem. Soc.* **2011**, *133*, 8846. (ab) Xu, Y.; Fischer, A.; Duan, L.; Tong, L.; Gabrielsson, E.; Åkermark, B.; Sun, L. *Angew. Chem., Int. Ed.* **2010**, *49*, 8934. (ac) Kärkäs, M.; Åkermark, T.; Johnston, E.; Karim, S.; Laine, T.; Lee, B.-L.; Åkermark, T.; Privalov, T.; Åkermark, B. *Angew. Chem., Int. Ed.* **2012**, *51*, 11589.

(3) (a) Barnett, S. M.; Goldberg, K. I.; Mayer, J. M. *Nat. Chem.* **2012**, *4*, 498. (b) Zhang, M.-T.; Chen, Z.; Kang, P.; Meyer, T. J. *J. Am. Chem. Soc.* **2013**, *135*, 2048. (c) Chen, Z.; Meyer, T. J. *Angew. Chem., Int. Ed.* **2013**, *52*, 700.
(4) (a) Yagi, M.; Wolf, K. V.; Baesjou, P. J.; Bernasek, S. L.; Dismukes, G. C. *Angew. Chem., Int. Ed.* **2001**, *40*, 2925. (b) Najafpour, M.; Ehrenberg, T.; Wiechen, M.; Kurz, P. *Angew. Chem. Int. Ed.* **2010**, *49*, 2233. (c) Poulsen, A. K.; Rompel, A.; McKenzie, C. J. *Angew. Chem. Int. Ed.* **2005**, *44*, 6916. (d) Kurz, P. *Dalton Trans.* **2009**, 6103. (e) Gao, Y.; Åkermark, T.; Liu, J.; Sun, L.; Åkermark, B. *J. Am. Chem. Soc.* **2009**, *131*, 8726. (f) Yagi, M.; Narita, K. *J. Am. Chem. Soc.* **2004**, *126*, 8084. (g) Hocking, R. K.; Brimblecombe, R.; Chang, L.-Y.; Singh, A.; Cheah, M. H.; Glover, C.; Casey, W. H.; Spiccia, L. *Nat. Chem.* **2011**, *3*, 461. (h) Limburg, J.; Vrettos, J. S.; Liable-Sands, L. M.; Rheingold, A. L.; Crabtree, R. H.; Brudvig, G. W. *Science* **1999**, *283*, 1524. (i) Karlsson, E.; Lee, B.-L.; Åkermark, T.; Johnston, E.; Kärkäs, M.; Sun, J.; Hansson, Ö.; Bäckvall, J.-E.; Åkermark, B. *Angew. Chem., Int. Ed.* **2011**, *50*, 11715.
(5) (a) Wasylenko, D. J.; Ganesamoorthy, C.; Borau-Garcia, J.; Berlinguette, C. P. *Chem. Commun.* **2011**, *47*, 4249. (b) Dogutan, D. K.; McGuire, R.; Nocera, D. G. *J. Am. Chem. Soc.* **2011**, *133*, 9178. (c) Kanan, M. W.; Nocera, D. G. *Science* **2008**, *321*, 1072. (d) Yin, Q.; Tan, J. M.; Besson, C.; Geletii, Y. V.; Musaev, D. G.; Kuznetsov, A. E.; Luo, Z.; Hardcastle, K. I.; Hill, C. L. *Science* **2010**, *328*, 342. (e) Rigsby, M. L.; Mandal, S.; Nam, W.; Spencer, L. C.; Llobet, A.; Stahl, S. S. *Chem. Sci.* **2012**, *3*, 3058. (f) Leung, C.-F.; Ng, S.-M.; Ko, C.-C.; Man, W.-L.; Wu, J.; Chen, L.; Lau, T.-C. *Energy Environ. Sci.* **2012**, *5*, 7903.
(6) (a) Fillol, J. L.; Codolà, Z.; Garcia-Bosch, I.; Gómez, L.; Pla, J. J.; Costas, M. *Nat. Chem.* **2011**, *3*, 807. (b) Ellis, W. C.; McDaniel, N. D.; Bernhard, S.; Collins, T. J. *J. Am. Chem. Soc.* **2010**, *132*, 10990. (c) Chen, G.; Chen, L.; Ng, S.-M.; Man, W.-L.; Lau, T.-C. *Angew. Chem., Int. Ed.* **2013**, *52*, 1789.
(7) (a) Duan, L.; Fischer, A.; Xu, Y.; Sun, L. *J. Am. Chem. Soc.* **2009**, *131*, 10397. (b) Duan, L.; Bozoglian, F.; Mandal, S.; Stewart, B.; Privalov, T.; Llobet, A.; Sun, L. *Nat. Chem.* **2012**, *4*, 418. (c) Duan, L.; Araujo, C. M.; Ahlquist, M. S. G.; Sun, L. *Proc. Natl. Acad. Sci. U.S.A.* **2012**, *109*, 15584. (d) Wang, L.; Duan, L.; Stewart, B.; Pu, M.; Liu, J.; Privalov, T.; Sun, L. *J. Am. Chem. Soc.* **2012**, *134*, 18868.
(8) (a) Gilbert, J. A.; Eggleston, D. S.; Murphy, W. R., Jr.; Geselowitz, D. A.; Gersten, S. W.; Hodgson, D. J.; Meyer, T. J. *J. Am. Chem. Soc.* **1985**, *107*, 3855. (b) Che, C. M.; Tang, W. T.; Wong, W. T.; Lai, T. F. *J. Am. Chem. Soc.* **1989**, *111*, 9048. (c) Collins, T. J.; Gordon-Wylie, S. W. *J. Am. Chem. Soc.* **1989**, *111*, 4511.
(9) Chen, Z.; Concepcion, J. J.; Luo, H.; Hull, J. F.; Paul, A.; Meyer, T. J. *J. Am. Chem. Soc.* **2010**, *132*, 17670.
(10) Dulière, E.; Devillers, M.; Marchand-Brynaert, J. *Organometallics* **2003**, *22*, 804.
(11) Palatinus, L.; Chapuis, G. *J. Appl. Crystallogr.* **2007**, *40*, 786.
(12) Farrugia, L. J. *J. Appl. Crystallogr.* **1999**, *32*, 837.
(13) Sheldrick, G. *Acta Crystallogr., Sect. A: Found. Crystallogr.* **2007**, *64*, 112.